



Cite this: *RSC Appl. Polym.*, 2024, **2**, 945

## A direct comparison of the thermal reprocessing potential of associative and dissociative reversible bonds in thermosets†

Arijana Susa, \* Willem Vogelzang, Wouter Teunissen, Karin Molenveld, Evelien Maaskant and Wouter Post

This study compares the thermal reprocessing potential of thermosets comprising associative or dissociative dynamic covalent bonds by evaluating their rheological behavior. In correspondence with earlier studies, it is shown that the dynamic behavior upon the application of a thermal stimulus is highly dependent on the selected molecular mechanisms. However, so far it has been difficult to unambiguously determine the effect of the type of reversible molecular mechanism on the reprocessing potential due to the significant dissimilarity of backbones within different thermosets. To overcome this hurdle, we designed and synthesized special model thermoset systems with near-identical backbones. This made it possible to assess the thermal reprocessing potential of these mechanisms directly and in a quantitative manner. A vinylogous urethane-based linkage and a Diels–Alder (DA) linkage were selected as the model associative and dissociative dynamic mechanisms, respectively. These linkages were embedded in comparable molecular structures, polymerized and subjected to near-identical processing conditions. The results show that the viscosity of a thermoset containing dissociative linkages can be severely reduced by applying heat, which could allow for more facile mechanical recycling *via* conventional thermoplastic processing methods. A similar impact on the viscosity was not observed in the associative thermoset prepared in this work and therefore the thermal reprocessing potential of this material is currently limited compared to its dissociative counterpart.

Received 9th November 2023,  
Accepted 26th July 2024

DOI: 10.1039/d3lp00242j  
[rsc.li/rscapplpolym](http://rsc.li/rscapplpolym)

## 1. Introduction

Thermoset polymers are characterized by the presence of covalent intermolecular cross-links. These linkages increase the material stiffness and strength and reduce the susceptibility to creep in comparison with thermoplastic polymers. This means that thermosets have good resistance to mechanical, thermal and chemical induced damage whilst still being lightweight compared to the ceramic and metallic alternatives.<sup>1</sup> Therefore, thermoset polymers such as isocyanates, unsaturated polyesters, and epoxies are highly suitable to be used as matrix materials in structural composites in combination with (functional) particles or reinforcing fibres. However, the multicomponent nature of these materials together with the permanent covalent chemical linkages results in the fact that thermoset composites are very difficult, if not impossible, to recycle in a circular manner.<sup>2</sup> As a result, the majority of thermoset waste is currently being deposited

into landfills. Other industrial waste processing methods for thermoset materials are combustion or grinding into particles that can be used as filler materials in lower quality applications.<sup>3</sup> A number of thermoset composite combustion methods such as pyrolysis or fluidized-bed combustion are capable of retrieving the particles or reinforcing fibres of the material but do not allow for recycling of the thermoset resin as this is incinerated in the process.<sup>4,5</sup> To reach higher levels of circularity for thermosets and their composites, collection and recycling of both the polymer resin and the fillers or reinforcing fibres is required.

As opposed to thermosets, thermoplastic polymers are much easier to recycle and can be recycled theoretically in very high yields multiple times. The key characteristic that allows for the mechanical recycling of thermoplastic materials is sufficient polymer chain mobility and flow (*i.e.* melting) at elevated temperatures, which makes reprocessing and reshaping of thermoplastic products possible. Two main differences between thermosets and thermoplastics regarding viscoelasticity are that (A) above the glass transition temperature ( $T_g$ ), thermoplastics show a certain temperature-dependent relaxation time with fluid behaviour at long times and elastic behaviour at short times, while thermosets maintain solid

Wageningen Food and Biobased Research, Wageningen University and Research, P.O. Box 17, 6700 AA Wageningen, the Netherlands. E-mail: [rijana.susa@wur.nl](mailto:rijana.susa@wur.nl)  
† Electronic supplementary information (ESI) available. See DOI: <https://doi.org/10.1039/d3lp00242j>



“elastic” behaviour at all accessible times and temperatures and (B) the order of magnitude of the stress relaxation modulus above the glass transition is lower for thermoplastics (of order 1 MPa or below depending on the chemistry) than for thermosets (between 1 and 100 MPa depending on the chemistry and crosslinking density). These differences are directly linked to the processability of thermoplastics (A) and the superior mechanical properties and stability of thermosets (B). Studies on the viscoelasticity and polymer dynamics of novel materials with reversible interactions are therefore important as they provide a direct assessment of the mechanical properties, relaxation and (re)processability.<sup>6</sup>

Alternative types of covalent bonds have been explored in the past decades as a potential solution to overcome the poor recyclability of thermosets. They can be sorted into dynamic and degradable covalent bonds. Dynamic covalent bonds enable temporary molecular mobility in a thermoset polymer upon the application of an external stimulus which can be of thermal, chemical or optical nature.<sup>1,7</sup> When a stimulus is removed, the cross-links are restored. In the past decades, many different dynamic covalent chemistries were reported including Diels–Alder,<sup>8,9</sup> disulfide<sup>10,11</sup> and polyimine exchange<sup>12,13</sup> and transesterification reactions.<sup>14,15</sup> Degradable linkages (e.g. acetal bonds), which can also be used to induce recyclability into thermoset resins, will not revert the material back to its original composition and therefore will require a larger recycling loop in order to provide a circular solution. While the difference in recyclability between degradable and dynamic molecular linkages becomes directly apparent upon comparison of the thermal reprocessing output (Fig. 1a), its impact on the recycling potential of different types of dynamic covalent linkages is less prominent.

Significant differences in the mechanisms of different dynamic covalent bonds but their influence on practical application are hardly studied.<sup>16</sup> In general, dynamic covalent linkages can be divided into associative and dissociative linkages and

their impact on the thermal reprocessing, and therefore recycling potential of a thermoset, is hypothesized to be substantial.<sup>2</sup> Associative dynamic covalent adaptable networks (ADCANS), also known as vitrimers, are based on the simultaneous exchange of one reactive site with another, in which the original cross-link is only broken when a new covalent bond has formed.<sup>17,18</sup> This can also be envisioned as a more fixed crosslinking density during bond exchange.<sup>19</sup> On the other hand, dissociative linkages of dissociative dynamic covalent adaptable networks (DDCANS) actually yield the temporary presence of two unlinked reactive sites prior to rebonding. This means that a decrease in crosslinking density is proportional to the loss in network connectivity.<sup>20</sup> A schematic representation of the associative and dissociative linkages is given in Fig. 1a.

At higher temperatures, determined by the so-called ‘topology freezing temperature’,  $T_v$ , the viscosity of vitrimers is controlled by chemical exchange reactions, resulting in a thermal viscosity decrease that follows the Arrhenius law.<sup>15,18</sup> Above  $T_v$ , exchangeable reactions happen fast and the vitrimer should be able to be reprocessed and recycled. Below  $T_v$ , exchangeable reactions are slow and the vitrimer is similar to a traditional thermoset.  $T_v$  not only determines the upper limit usage temperature for a vitrimer, but also has a direct impact on the vitrimer’s performance and reprocessing. Even though the  $T_v$  enables a certain viscosity drop to make those thermosets soften, obtaining viscosity levels that allow for conventional thermoplastic processing (e.g. *via* injection moulding or extrusion) remains a challenge. There are several examples of processable vitrimers reported,<sup>21–25</sup> but this success usually comes with a sacrifice of their properties. For example, varying the crosslinking density modifies the viscosity and creep resistance of the vitrimer both at room and elevated temperatures, but this results in a decreased  $T_g$  and inadequate tensile properties. A successful example of improving this limitation was shown by Guerre *et al.* who have developed a vitrimer with dual relaxation behaviour.<sup>26</sup>

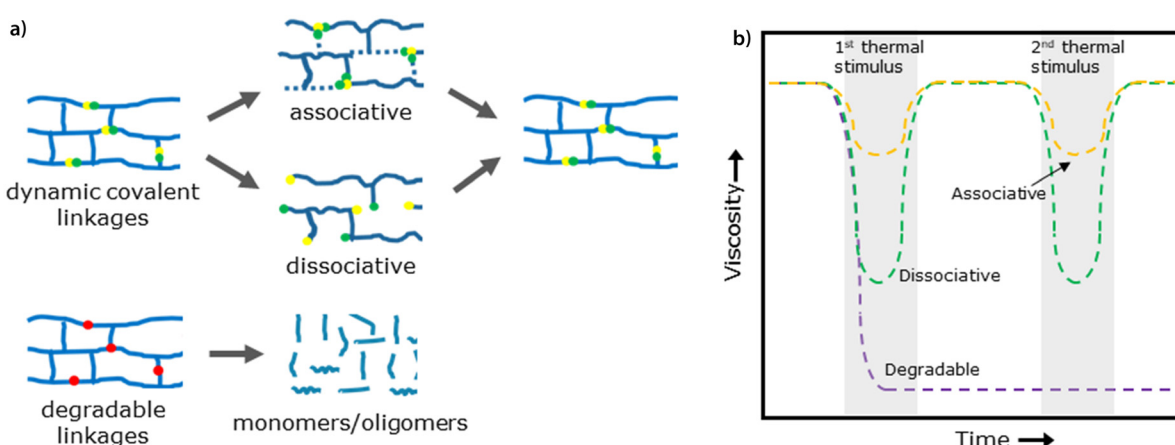


Fig. 1 (a) Schematic representation of associative, dissociative and degradable linkages in a thermoset network when applying a thermal stimulus. Only dissociative and associative linkages can reform a cross-linked network, whereas degradable linkages will result in the formation of monomers or oligomers. (b) Graphical representation of the theoretical viscosity as a function of time when applying a thermal stimulus to associative, dissociative and degradable linkages.



DDCANs and thermoplastic materials are different because these materials transition from a solid to a liquid state in a much more discernible way, following the Williams–Landel–Ferry model (WLF) for thermoplastic polymer melts.<sup>15</sup> Therefore it is theorized that dissociative networks are more capable of reaching the on-demand viscosity drop that is necessary for effective composite component separation required for thermal reprocessing *via*, for example, extrusion. This could give dissociative networks a distinct advantage over associative networks. This hypothetical relationship between the thermoset viscosity and the applied thermal stimulus of associative, dissociative and degradable linkages is schematically depicted in Fig. 1b.

Unfortunately, it is rather complex to compare the thermal reprocessing potential of ADCANs and DDCANs quantitatively as they are typically built out of non-identical complex molecular structures designed to deliver specific material properties tailored towards the functional requirements of thermoset containing products. In addition, the thermoset processing operations and measurement techniques, which largely impact the reported static and dynamic material properties, tend to be different from facility to facility and this complicates a thorough comparison. To overcome this, this study aims to offer a direct comparison of the thermal dynamic behaviour and thereby the thermal reprocessing potential of the associative and dissociative dynamic covalent bonds. This was achieved by designing and synthesizing both associative and dissociative model thermosets with near-identical molecular network structures. A vinylogous urethane (VU) linkage and a Diels–Alder (DA) linkage were selected as the model associative and dissociative dynamic mechanisms, respectively. These linkages were embedded in highly comparable molecular structures and subjected to near-identical processing conditions. This enabled an objective comparison of the potential of these two different molecular mechanisms to be reprocessed *via* methods that require a low polymer viscosity such as polymer extrusion.

## 2. Experimental section

### 2.1. Chemicals

1,1,1-Tris(hydroxymethyl)propane (TMP, 97%), acetic anhydride (>99%), sodium acetate anhydrous (>99%), *tert*-butyl acetoacetate (98%), 3-(2-furyl)propionic acid (97%), dimethylsulfoxide-d<sub>6</sub> (DMSO-d<sub>6</sub>, 99.8%D), and chloroform-d (CDCl<sub>3</sub>, 99.8%D) were obtained from Sigma-Aldrich, the Netherlands. Maleic anhydride (>99%) and 1,2-bis(2-aminoethoxy)ethane (>98%) were obtained from TCI Europe. THF (>99%) was obtained from VWR, the Netherlands. All chemicals were used as received.

### 2.2. Monomer synthesis

**Synthesis of bismaleimide.** The synthesis of bismaleimide was based on literature procedures.<sup>27,28</sup> 1,2-Bis(2-aminoethoxy)ethane (26.68 g, 0.22 mol) was added dropwise to a stirring

cooled solution (0–5 °C) of maleic anhydride (0.063 mol) in dichloromethane (180 mL). Next, the mixture was stirred for 3 hours at room temperature. Filtration over a glass filter type 3 gave the corresponding bismaleamic acid as a white solid material (88% yield). The bismaleamic acid (80 g, 0.26 mol) and sodium acetate (27.2 g, 0.34 mol) were added to acetic anhydride (500 mL). The mixture was heated at reflux (110 °C) for 3 hours. The resulting brownish colored solution was poured into stirring ice-water (1000 mL) and the intended product was extracted with chloroform (3 × 500 mL). The organic layers were combined and washed with water, an aqueous solution of NaHCO<sub>3</sub> (1 × 500 mL) and again water (500 mL). Next, the organic phase was evaporated to dryness yielding a brownish solid (33.20 g, 32.9%). <sup>1</sup>H NMR (400 MHz, CDCl<sub>3</sub>) δ 6.73 (s, 4H), 3.70 (s, 4 H), 3.56 (d, 8 H). <sup>13</sup>C NMR (101 MHz, CDCl<sub>3</sub>) δ 170.66, 134.14, 69.93, 67.74, 37.06.

**Synthesis of trifuran.** A 100 mL 3-neck round bottom flask was equipped with a Buchi bmd 075 magnetic coupling with Teflon stirrer blades, a distillation set-up and a collection flask. 1,1,1-Tris(hydroxymethyl)propane (1.52 g, 11.2 mmol) and 3-(2-furyl)propionic acid (9.37 g, 67.4 mmol, 6 eq.) were added and the mixture was heated to 165 °C. Soon the color of the melt turned from deep yellow into amber, and after the temperature was raised to 220 °C. The reaction was run for 8 hours in total. The excess of furanic compound was removed under high vacuum (160 °C, 2 × 10<sup>-1</sup> mbar), yielding a brown oil (5.75 g, 103%). It should be noted that the yield was >100% due to residual 3-(2-furyl)propionic acid after vacuum distillation.

<sup>1</sup>H NMR (400 MHz, CDCl<sub>3</sub>) δ 7.28 (s, 3H), 6.25 (q, *J* = 2.5 Hz, 3H), 6.00 (d, *J* = 3.3 Hz, 3H), 3.99 (s, 6H), 2.94 (t, *J* = 7.6 Hz, 6H), 2.71–2.57 (m, 6H), 1.39 (q, *J* = 7.6 Hz, 2H), 0.82 (t, *J* = 7.5 Hz, 3H). <sup>13</sup>C NMR (101 MHz, CDCl<sub>3</sub>) δ 172.25, 153.82, 141.29, 110.23, 105.39, 63.85, 40.65, 32.39, 23.36, 23.10, 22.75, 7.23.

**Synthesis of trisacetoacetate.** A 500 mL 3-neck round bottom flask was equipped with a Buchi bmd 075 magnetic coupling with Teflon stirrer blades. Trimethylolpropane (29.92 g, 0.22 mol, 1.000 eq.) and *tert*-butyl acetoacetate (219 mL, 1.332 mol, 5.98 eq.) were introduced into the flask. The biphasic mixture was heated to 150 °C (temperature internally measured), after which the mixture became homogeneous. After approximately 30 minutes, the by-product *tert*-butanol was collected. The reaction was prolonged for 16 hours at 150 °C and then the excess of *tert*-butyl acetoacetate was removed under high vacuum (~2 mbar).<sup>29</sup> The product was obtained as a slightly viscous pale-yellowish oil (86.26 g, 0.22 mol, 99.8%).

<sup>1</sup>H NMR (400 MHz, CDCl<sub>3</sub>) δ 4.04 (s, 6H), 3.44 (s, 6H), 2.21 (s, 9H), 1.46–1.40 (q, *J* = 7.6, 2H), 0.86–0.82 (t, *J* = 7.5 Hz, 3H). <sup>13</sup>C NMR (101 MHz, CDCl<sub>3</sub>) δ 200.26, 166.76, 64.36, 49.78, 40.81, 30.24, 22.84, 7.23.

### 2.3. Thermoset synthesis

The vinylogous urethane (VU, associative) thermoset was prepared by mixing diamine (1.65 eq.) and trisacetoacetate (1 eq.) in a stoichiometric ratio of 0.90 [(equivalent acetoacetate)/



(equivalent amine)] for 2 minutes at 2000 rpm. Subsequently, the material was post-cured between two Teflon sheets in a stainless steel mould for 30 minutes at 150 °C (20 tons) using a hydraulic press (PHI, type 75U1209S-2JCS-J-Y2-S5-7).

The Diels–Alder (DA, dissociative) thermoset was prepared by mixing bismaleimide (3 eq.) and tris-furan (2 eq.) in a Speed mixer® DAC 150.1 FVZ and placed inside a pre-heated oven for 10 minutes at 150 °C to homogenize the components. Next, the brownish liquid was mixed in a Speed mixer® DAC 150.1 FVZ for 2 minutes at 2000 rpm. Subsequently, the material was post-cured in an oven for 30 minutes at 150 °C.

#### 2.4. Characterization

Nuclear magnetic resonance (NMR) spectra were recorded on a Bruker Avance III 400 MHz spectrometer operating at 400.17 MHz ( $^1\text{H}$ ) and 100.62 MHz ( $^{13}\text{C}$ ). The system includes an inverse broadband probe fitted with a Z-axis gradient and with automatic tuning and matching. Proton NMR chemical shifts are quoted in parts per million (ppm) referenced to the appropriate solvent peak. Carbon NMR was fully decoupled by broad band decoupling.

Fourier transform infrared (FTIR) spectra were recorded in attenuated total reflectance (ATR) mode on a Bruker Alpha 2 spectrometer equipped with a diamond crystal in the spectral range from 4000 to 650  $\text{cm}^{-1}$  with a resolution of 4  $\text{cm}^{-1}$ . The number of scans for each spectrum was set at 24. The spectrometer was operated with OPUS software version 8.1.

Differential scanning calorimetry (DSC) measurements were performed using a PerkinElmer DSC 8000 provided with liquid nitrogen cooling and an auto sampler. Stainless steel DSC cups with rubber rings were used. Samples were heated from 0 to 150 °C with a heating and cooling rate of 10 °C  $\text{min}^{-1}$ .

The rheology experiments were performed on cured disc-shaped specimens with a radius of 10 mm using an Ares G2 rheometer equipped with a 10 mm serrated plate on a 25 mm serrated plate for the vitrimer material or a disposable 25 mm stainless steel plate on a 42 mm cup for the Diels–Alder material. Vitrimer specimens were conditioned for 2 minutes at 150 °C under an axial force of 10 N. This axial force was lowered to 0.1 N before starting the desired program. Due to the lower viscosity when compared to vitrimers, Diels–Alder specimens were heated without the axial force to 150 °C for two minutes and then compressed to the desired gap of 1 mm. Temperature sweeps were performed from 230 °C (vitrimer) and 160 °C (Diels–Alder) down to –50 °C at 5 °C  $\text{min}^{-1}$  cooling speed. The dissociative thermoset requires a heating temperature of 150 °C to have a full rDA conversion. In contrast, the VU thermoset requires a lower temperature of 115 °C to show reversible behaviour. For both thermosets, we kept the heating rate constant at 10 °C  $\text{min}^{-1}$  because thermal responses are typically heating rate dependent. Due to this constant heating rate, the heating (and cooling) of the dissociative thermoset took longer than that of the associative thermoset, and therefore the holding time for the associative thermoset was set longer in order to have a similar overall heating cycle time. The dynamic frequency was 1 Hz and the sampling interval

was 1 pt  $\text{s}^{-1}$ . The automatic axial force was 0.1 N ( $\pm 0.02$  N) for the measurements of vitrimers and 0 N ( $\pm 0.02$  N) for that of the Diels–Alder samples to prevent gap closure and sample leakage when the sample was in the liquid phase. Automatic strain was used to prevent non-linear stress behaviour but allow a good signal/noise response in lower stiffness regions. The strain range was 0.001% to 1% and steered by the torque in the range of 10  $\mu\text{N m}$  to 200  $\mu\text{N m}$ . When a strain sweep was performed, no autostrain was applied.

Swelling and solubility tests were performed in triplicate. A piece of the cured thermoset (35–55 mg) was immersed in 3 mL THF for 24 h at room temperature while placed on an orbital shaker (IKA KS 125 basic). Next, the solvent was removed and the samples were dried under vacuum until a constant weight was reached. The swelling degree was calculated using eqn (1) and the gel fraction was calculated using eqn (2).

$$\text{Swelling degree}(\%) = \frac{M_{\text{swollen}} - M_{\text{initial}}}{M_{\text{initial}}} \times 100\% \quad (1)$$

$$\text{Gel fraction}(\%) = \frac{M_{\text{dried}}}{M_{\text{initial}}} \times 100\% \quad (2)$$

where  $M_{\text{initial}}$ ,  $M_{\text{swollen}}$ , and  $M_{\text{dried}}$  are the initial, swollen and dry mass, respectively.

## 3. Results and discussion

### 3.1. Molecular analysis of thermoset structures and functionality

Associative and dissociative thermoset networks with near-identical backbones were prepared by functionalizing ethylene glycol (a bifunctional monomer) and trimethylolpropane (a trifunctional monomer) with the desired reactive groups. The associative thermoset was prepared from a diamine and trisacetoacetate, yielding VU linkages. The dissociative thermoset was prepared from a bismaleimide and trisfuran, yielding DA linkages. Fig. 2a and b show the chemical structures of the monomers and the resulting VU and DA linkages, respectively. The molecular changes that occur during thermal reprocessing are shown at the bottom of Fig. 2, clearly depicting the key difference between the two thermosets: while the dissociative mechanism results in complete de-bonding of the polymer backbone, the associative thermoset retains constant cross-linking density due to the associative exchange reactions.

The successful conversion of the monomers into the thermoset network for both the associative and dissociative thermosets was shown by Fourier transform infrared (FTIR) measurements. Fig. 3a shows the FTIR spectra of the individual monomers and the cured associative VU thermoset. The trisacetoacetate shows two signals at 1739 and 1711  $\text{cm}^{-1}$  that could be attributed to the ester and ketone bands of the acetooacetate groups, respectively. In the cured associative thermoset, these vibrations are replaced by signals at 1642  $\text{cm}^{-1}$  and 1594  $\text{cm}^{-1}$  which can be attributed to the carbonyl (C=O) and



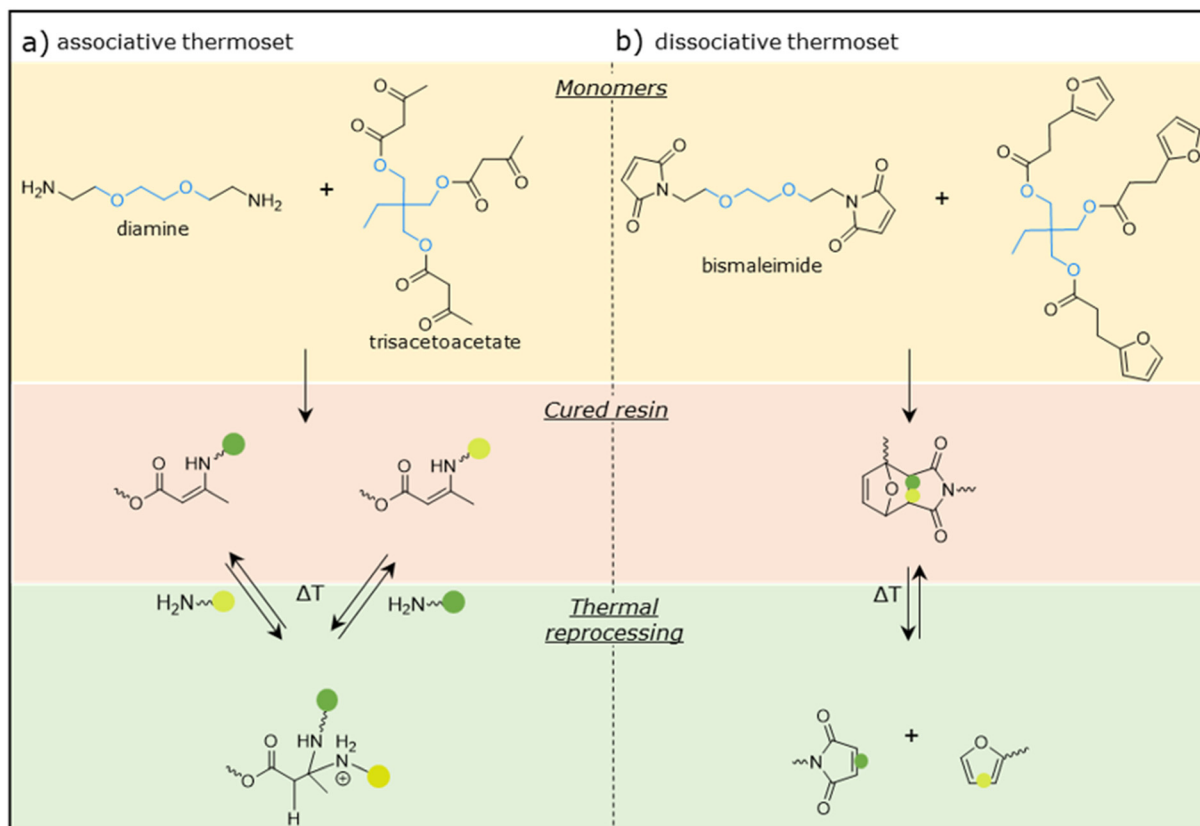


**Fig. 2** (a) Synthesis of the associative thermoset based on a diamine and trisacetoacetate yielding a resin with vinylogous urethane linkages. (b) Synthesis of the dissociative thermoset based on bismaleimide and trifuran yielding a resin with DA linkages. The respective reversible mechanisms responsible for the thermal reprocessability are depicted at the bottom.

C=C bands of the vinylogous urethane linkage, respectively, showing (almost) full conversion.<sup>30</sup>

Similarly, full conversion of the monomers into the dissociative network was observed, as shown in Fig. 3b. The characteristic signals of the maleimide group at 3097, 831 (C–H), and 694 (ring bending)  $\text{cm}^{-1}$  are not present in the cured dissociative DA thermoset.<sup>31</sup> New signals at 1774 (C=O) and 1185 (C–N–C)  $\text{cm}^{-1}$  are attributed to the succinimide ring in the DA adduct.<sup>32</sup>

In addition, swelling tests were performed to calculate the swelling degree and the gel fraction of the thermosets (Table 1). The associative and dissociative thermosets show average swelling degrees of 94% and 45%, respectively. Furthermore, the gel fraction was found to be almost 100% in both the associative and dissociative thermosets (99% and 97%, respectively). Thus, based on these swelling tests it can be concluded that for both thermosets an almost full conversion of the monomers into a cross-linked structure was obtained, which is in agreement with the ATR-FTIR results. Because of the (almost) full monomer conversion, it is unlikely that the differences in the swelling degree originate from a significant difference in the crosslinking density between the thermosets. Most likely these differences can be attributed to the lower affinity of the dissociative thermoset for the solvent tetrahydrofuran.

The thermal properties of the cured thermosets were evaluated with thermogravimetric analysis (TGA, see ESI Fig. S1†) and differential scanning calorimetry (DSC). Fig. 4 shows the DSC thermograms of five heating cycles for the associative and dissociative thermosets. Both thermosets show a very similar glass transition temperature ( $T_g$ ) of 43 °C and 45 °C for the associative and dissociative thermosets, respectively. These similar glass transition temperatures can be explained by the similarities in the chemical backbone of the thermosets, contributing thus to the comparability of the two thermosets. The associative thermoset does not show other thermal transitions up to 150 °C, as the so-called topology freezing temperature ( $T_v$ ) cannot be observed by DSC.<sup>33</sup> In contrast, the retro Diels–Alder (rDA) reaction is endothermic and thus can be observed by DSC. As shown in Fig. 4b, two broad transitions are observed which can be attributed to the two diastereoisomers that are formed in a DA reaction: the endo-adduct and the exo-adduct.<sup>34</sup> The exo-adduct is thermally more stable than the endo-adduct, resulting in a higher rDA temperature. Thus the first transition around 105 °C is attributed to the rDA reaction of the endo-adduct and the second transition around 137 °C is attributed to the rDA reaction of the exo-adduct. Hot stage FTIR measurements of the cured thermoset (see ESI Fig. S3†) show little changes in the FTIR spectrum of the thermoset at



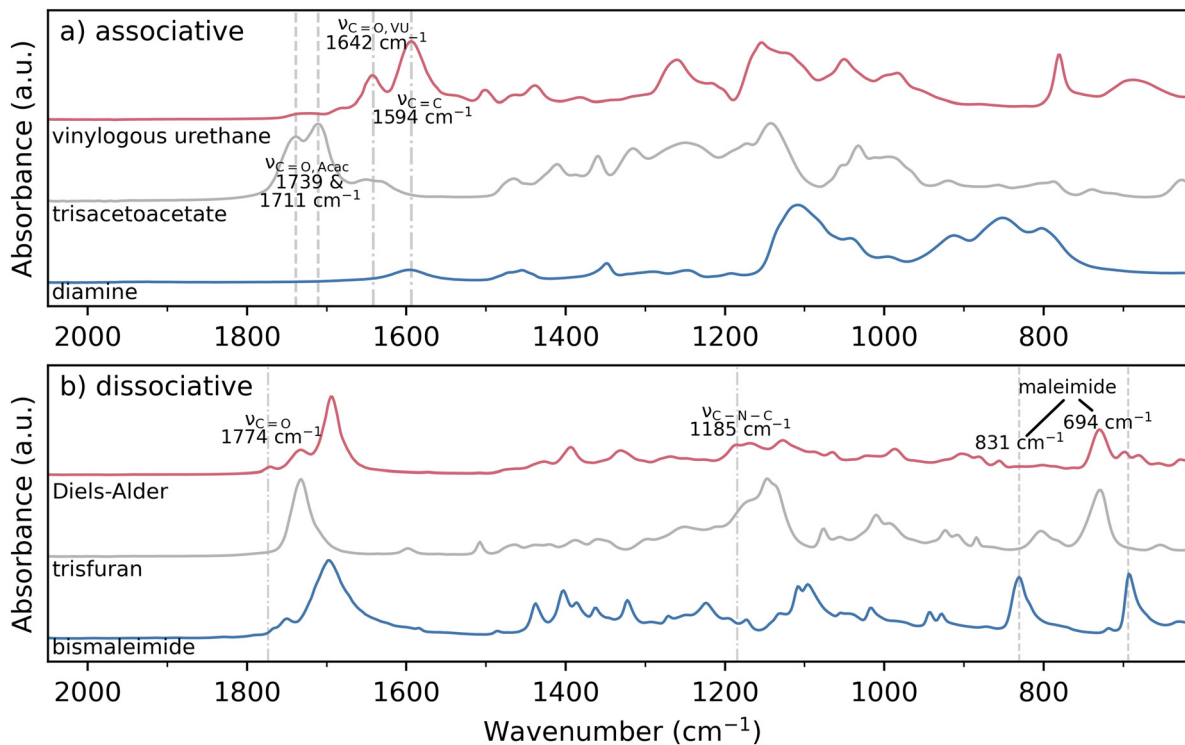


Fig. 3 Magnified ATR-FTIR spectra of the monomers and the cured thermosets recorded at room temperature. (a) Trisacetoacetate and the cured vinylogous urethane thermoset. (b) Bismaleimide, trifuran, and the cured DA thermoset. The full scale spectra can be found in ESI Fig. S2.†

Table 1 Swelling degree and the soluble fraction of the thermosets

CAN	Swelling degree <sup>a</sup> (%)	Gel fraction <sup>b</sup> (%)
Associative	94 ± 4	99 ± 0.1
Dissociative	48 ± 11	97 ± 2

<sup>a</sup> Determined after 24 h in THF *via* eqn (1). <sup>b</sup> Determined *via* eqn (2) after 24 h in THF and dried for 24 h in a vacuum oven at 40 °C.

80 °C when compared to the room temperature spectrum, whereas at 120 °C (the upper limit of the hot stage), a clear increase of the maleimide signal at 831 cm<sup>-1</sup> is observed, which is an indication of the rDA reaction. On the other hand, the succinimide ring signals at 1774 and 1185 cm<sup>-1</sup> are still present at 120 °C, albeit with a slightly lower intensity. Thus, a full conversion of the rDA reaction is not achieved at 120 °C, which can be attributed to the presence of the exo-adduct which is favourable at higher temperatures, as shown in the DSC thermograms in Fig. 4b. To confirm the full conversion of the rDA reaction of the exo-adduct at 150 °C, a piece of the dissociative thermoset was dissolved in DMSO-d<sub>6</sub> by heating for 30 minutes at 150 °C. Next, the sample was cooled to room temperature and a <sup>1</sup>H-NMR spectrum was recorded (see Fig. 5). It can be concluded that the spectrum is a sum of individual monomers, and hence a full conversion of the rDA reaction was observed.

The thermal stability of the thermosets was assessed by DSC by reheating the same sample five consecutive times. As

shown in Fig. 4, the  $T_g$  of both the associative and dissociative thermosets does not change significantly with increasing heating cycle. However, the enthalpy of the endo rDA transition drops from 3.4 J g<sup>-1</sup> in the first heating cycle to 1.9 in the second heating cycle and drops further to 1.6 J g<sup>-1</sup> in the subsequent heating cycles (see Table S1† for the integrals for all five consecutive heating treatments), whereas the enthalpy of the exo rDA transitions stays constant at around 3.1 J g<sup>-1</sup> during subsequent heating cycles. Similar observations were made by Ehrhardt *et al.* who attributed this drop in endo rDA reaction enthalpy to a lower crosslinking density as the time between the subsequent DSC heating cycles was not sufficient for the specimen to fully recover.<sup>35</sup>

### 3.2. Thermal response and stimulus determination of model thermosets

The dynamic response of both the associative and dissociative model thermosets upon a gradual increase of temperature as measured by oscillatory shear rheology is depicted in Fig. 6. Four distinctive regions are visible upon heating the dissociative thermoset. As seen in Fig. 6a, the first region is characterized by a plateau from -50 to 27 °C, where the polymer network is frozen in the glassy state with the storage modulus,  $G'$  – which characterizes the solid-like polymer behaviour – being higher than the loss modulus,  $G''$ , which characterizes the liquid-like polymer behaviour. It can be noticed that the associative polymer exhibits higher glassy moduli than the dissociative polymer. This is attributed to the intermolecular



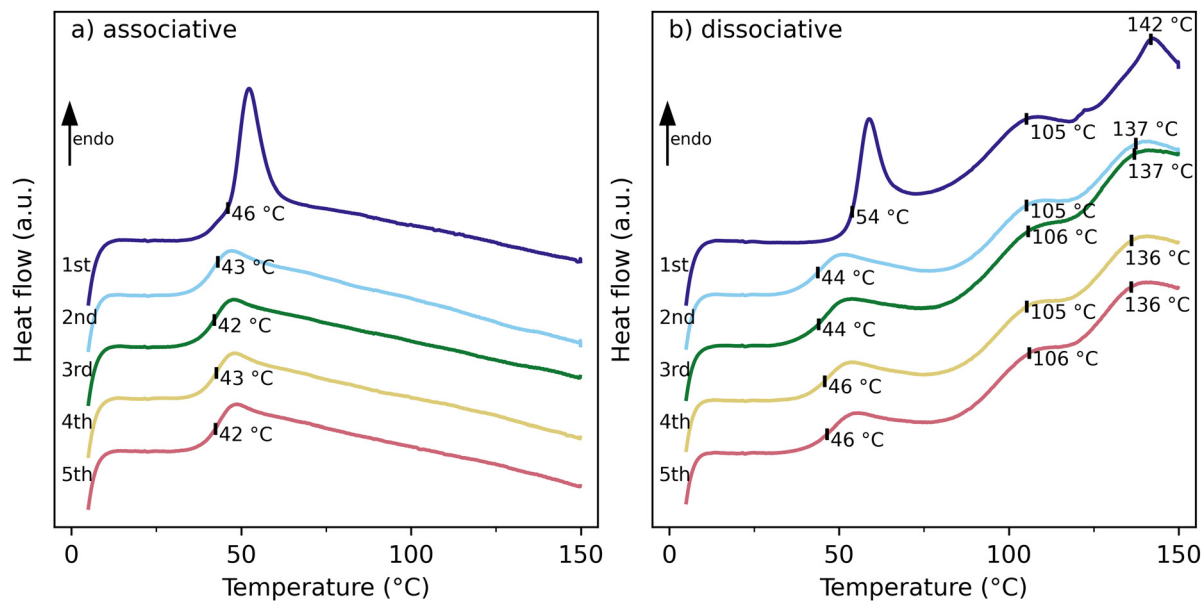


Fig. 4 DSC thermograms of (a) the associative (VU) and (b) dissociative (DA) specimens showing thermal behaviour during five consecutive heating treatments.

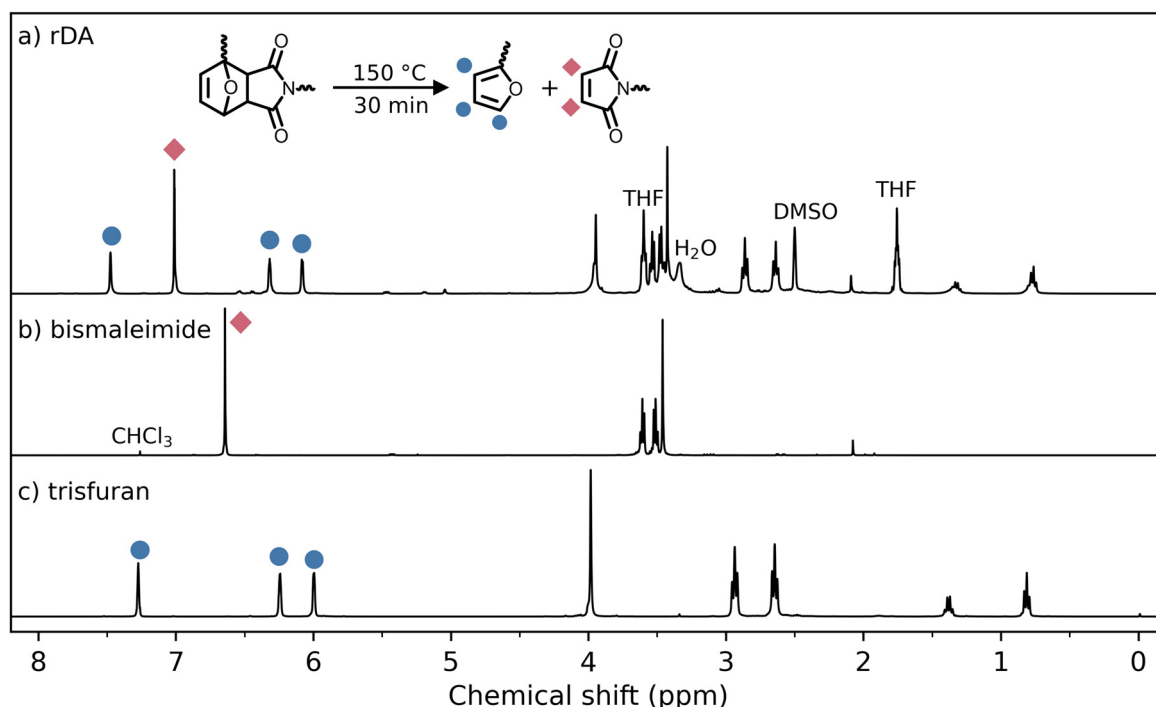
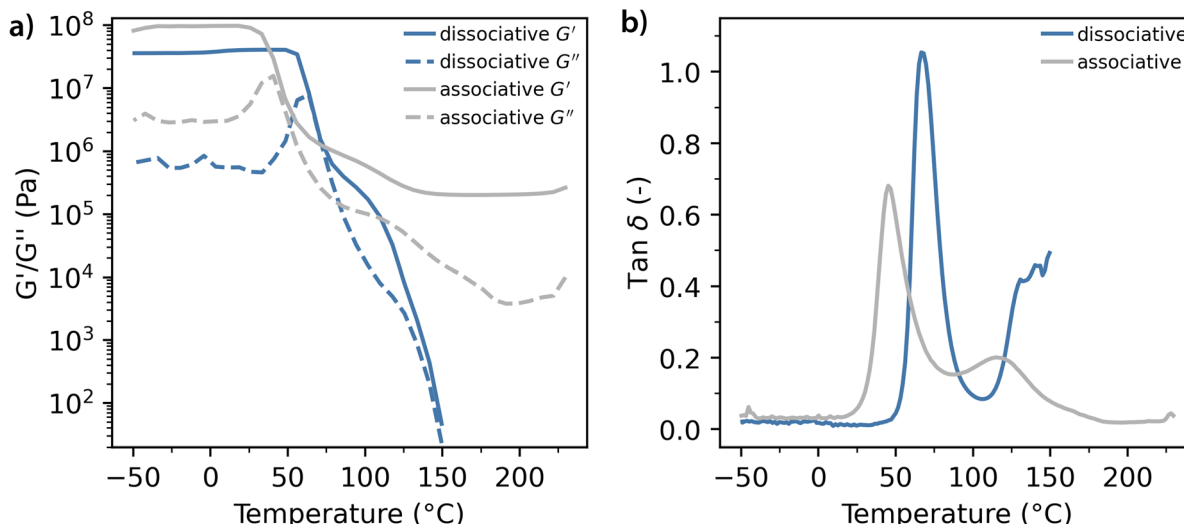


Fig. 5 <sup>1</sup>H-NMR spectra of (a) the DA-adduct after 30 minutes at 150 °C in DMSO-d<sub>6</sub>, (b) the bismaleimide monomer recorded in CDCl<sub>3</sub> and (c) the trisfuran monomer recorded in CDCl<sub>3</sub>. The THF observed in spectrum (a) is attributed to residual THF after the swelling tests.

NH...O hydrogen bonds within the VU network which can be formed prior to the curing and therefore contribute to a denser packing of the polymer chains in the cured state.<sup>36</sup> The second region starts with a sharp drop of both storage ( $G'$ ) and loss ( $G''$ ) moduli ranging from 60 to 75 °C. This is a typical relaxation that is observed at the glass transition point of any

polymer, which is also indicated by the peak in  $\tan(\delta)$ , which is the ratio of the loss over storage modulus, also called the damping coefficient, that is visible at 67 °C (Fig. 6b). The differences between the  $T_g$  as measured by DSC are around 10–12 °C and this is a common consequence of the differences in the measuring methods and heating rates.<sup>37</sup> The glass tran-





**Fig. 6** Temperature-dependent dynamic behaviour of the model dissociative (blue lines) and associative (grey lines) thermosets. (a) Storage ( $G'$ ) and loss ( $G''$ ) moduli; (b)  $\tan(\delta)$ .

sition region is characterized by the dominance of the liquid component over the solid component of the polymer with  $G' < G''$  and  $\tan(\delta) > 1$ . After this transition, the third region appears where  $G' > G''$  and  $\tan(\delta) < 1$  with the solid phase being dominant over the liquid one. Here the moduli decrease non-linearly with temperature, forming an elastic plateau and confirming a typical behaviour of dissociative networks and the absence of the sol-gel transition.<sup>38</sup> The fourth thermal transition region where  $G' \approx G''$  and  $\tan(\delta)$  increases is found within the 115–150 °C temperature range. This indicates a fourth relaxation step similar to what is commonly observed in thermoplastic materials (*i.e.* polymer melting) and does not exist in conventional thermosets. This transition is attributed to the thermally induced unlinking of covalent bonds due to the rDA reaction which is accompanied by severe softening and viscosity reduction of the polymer. This region continues to at least 150 °C while the storage and loss moduli have reached their measurable limit at this point. In accordance with the DSC results, 150 °C is confirmed to be the optimal reprocessing temperature ( $T_{rec}$ ) for the model dissociative thermoset.

The dynamic response of the associative model thermoset upon a gradual increase of temperature is also depicted in Fig. 6a. Again, both  $G'$  and  $G''$  show an initial drop corresponding to the glass-to-rubber transition. However, the second transition, starting at 60 °C shows a response that is much more typical of thermoset polymers as both  $G'$  and  $G''$  reach a plateau value which indicates that no further relaxation can occur due to the presence of permanent covalent urethane cross-links. The dynamic behaviour of the associative linkages does show in the presence of a second  $\tan(\delta)$  peak at 115 °C (Fig. 6b) which is a unique feature called ‘topology freezing temperature’ ( $T_v$ ) for vitrimers.<sup>15,18</sup> Moreover, this is the optimal temperature to trigger the dynamic response, which is therefore used as the  $T_{rec}$  for the model associative thermoset material throughout the remainder of this work.

The differences in dynamic response that are observed upon comparing the dissociative and associative thermosets are an indication that the induced polymer softening upon the application of a thermal stimulus will be substantially impacted by the type of dynamic covalent bond. The extent of polymer softening is obvious from the  $G'$  values at the  $T_{rec}$ , as the dissociative system is able to reach the terminal flow with a very low modulus ( $10 \text{ Pa} < G' < 100 \text{ Pa}$ ), while the associative system has its lowest moduli with values in the order  $10^5 \text{ Pa} < G' < 10^6 \text{ Pa}$ . The extent of polymer relaxation can be read from the  $\tan \delta$  values (Fig. 6b) as well, where the higher the  $\tan \delta$ , the higher the liquid behaviour dominance at the  $T_{rec}$ . The  $\tan \delta (T_{rec}) = 0.5$  for the dissociative polymer and  $\sim 0.2$  for the associative polymer, indicating a more relaxed state of the dissociative polymer at the  $T_{rec}$ .

### 3.3. Thermal processing potential of model thermosets

In order to determine the difference in the thermal reprocessing potential between the model dissociative and associative thermosets, the complex viscosity was measured for both materials over three consecutive thermal heating cycles. Fig. 7a shows the temperature-viscosity dependency of the dissociative DA based thermoset. Upon increasing temperature, a very sharp viscosity drop of multiple orders of magnitude is observed to a level that corresponds to a low viscous liquid-like flow, and when the thermal stimulus is removed, the viscosity quickly returns to its original solid state. This response is observed for each consecutive thermal treatment although the extent of the viscosity drop is lowered with every cycle. This partial irreversibility might be explained by the formation of poly(maleimide) resulting from self-polymerization, even at a relatively low temperature of 150 °C, although this temperature can differ for different DA thermosets. This phenomenon is a known characteristic and disadvantage of this type of dissociative bond<sup>39,40</sup> and is also observed after prolonged storage



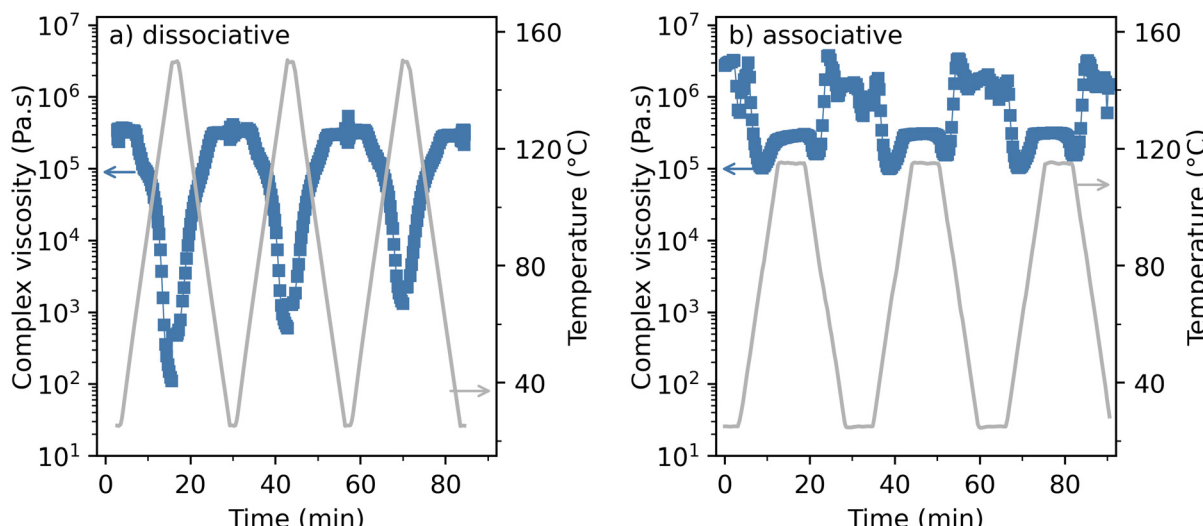


Fig. 7 Temperature–viscosity responses of (a) the dissociative (DA) and (b) associative (VU) model thermosets over 3 consecutive reprocessing cycles.

under ambient conditions. For the specific DA thermoset synthesized in this study it was found that after sample storage for approximately two years, low levels of irreversible cross-linking can have a major impact on the dynamic covalent response of the thermoset material (see Fig. S4 and S5 in the ESI†).

A similar thermal procedure was used to test the viscosity response of the model associative thermoset as depicted in Fig. 7b. This figure shows that a moderate drop in viscosity is observed upon heating the material. This viscosity drop is several orders of magnitude smaller than the one observed for the dissociative thermoset in Fig. 7a, which indicates a confirmation of the hypothesis postulated at the start of this study and by earlier theoretical work.<sup>2</sup>

In Fig. 7, it can be observed that upon the application of the temperature stimulus both the vinylogous urethane and the DA thermoset show a steep viscosity drop which is followed by an increase up to a certain plateau value. This effect could be attributed to a viscoelastic delay in the material response to the thermal stimulus caused by the rapid temperature increase in combination with instrument stabilization in between the applied thermal cycles. It is expected that a more gradual heating program would not show this initial minimum. Hence the complex viscosity values at the plateau levels are selected as the minimum viscosity values obtained.

The temperature–viscosity dependency of both thermosets developed in this study (as depicted in Fig. 7) shows a substantial difference in viscosity reduction that is obtained for the individual thermosets. Although the associative mechanism of the VU does show a viscosity drop, its minimum value does not reach values below  $10^5$  Pa s, which corresponds to a soft solid material.<sup>41</sup> The DA thermosets show a completely different response as the measured minimum complex viscosity ranges in each heating cycle reach a value of at least  $10^3$

Pa s, which corresponds to materials that are in a molten liquid state. Fig. 8 compares the viscosity response of both thermosets in a more illustrative manner. In this figure, the times of the performed experiments have been adjusted so that the application of the thermal stimulus is aligned for the three different heating cycles shown. This result is obtained by introducing an artificial time gap between the temperature ramps and the temperature isotherms of the applied rheology program.

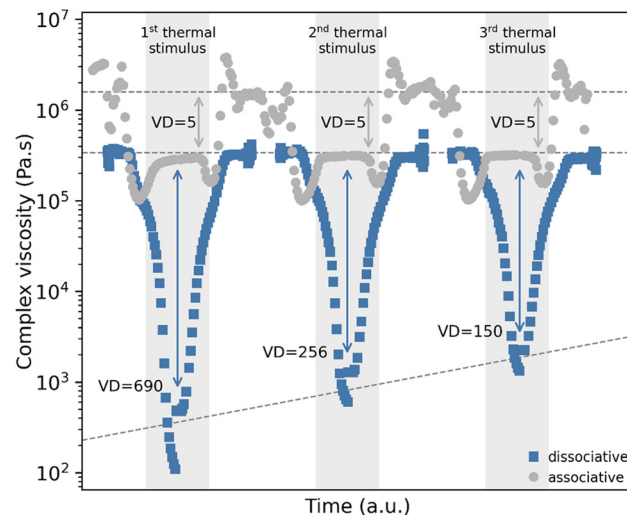


Fig. 8 Comparative analysis of the model vinylogous urethane and Diels–Alder thermosets developed in this study. The viscosity response is shown over the course of three thermal treatments (at 115 °C and 150 °C respectively). The time axis has been adjusted in order to align the thermal stimuli.



Fig. 8 shows that the viscous response of the two near-identical thermosets corresponds to the theoretical response that is hypothesized in Fig. 1. In order to quantify this difference in viscosity reduction the viscosity drop factor (VD) was introduced, which is calculated as:

$$VD_{\text{thermoset}} = \frac{\eta_{\text{complex-RT}}}{\eta_{\text{complex-ST}}} \quad (3)$$

where  $\eta_{\text{complex-RT}}$  is the complex viscosity before the application of a thermal stimulus and  $\eta_{\text{complex-ST}}$  is the minimum complex viscosity that is obtained during the application of the stimulus. The viscosity drop values for each of the three thermal treatments that are applied to the model thermosets are also shown in Fig. 8. These values show that, even though the minimum viscosity of the DA thermoset is increasing with each thermal treatment, the viscosity reduction remains more than two orders of magnitude higher than that of the VU thermoset. Thus, this result confirms the hypothesized theoretical behaviour of these materials described in Fig. 1 and recent articles published.<sup>2,42</sup> It is important to emphasize that this research has been performed on model systems. Hence, the absolute viscosity drop may depend on the exact chemical structure. The selected polymer backbones for these model molecular structures were deliberately chosen as small as possible in order to maximize the observed covalent response. Nevertheless, it is anticipated that this trend is valid for a wide range of chemical structures given the inherent chemical characteristics of dissociative and associative bonds. However, for more application oriented polymer networks with larger backbones and a subsequent lower concentration of dynamic covalent groups, the observed difference in the absolute viscosity drop between the two mechanisms may be less profound.

The results described in this study demonstrate that the thermal (re)processing potential of dynamic covalent thermosets with dissociative linkages is substantially higher than of those containing associative linkages. This difference is likely to have a high impact on the possibility of mechanically recycling of these thermoset resins and composites made thereof. Besides mechanical recycling and other reprocessing methods that require a low polymer viscosity, research is also performed on enabling the recyclability of thermosets *via* chemical recycling.<sup>2</sup> Still, mechanical recycling is considered to be the most preferred recycling route as it yields a higher level of material integrity compared to thermal and chemical recycling, and it results in energy and matter conservation. Although exceptions occur, for example, in some instances chemical recycling (e.g. solvolysis) might be a more preferred route. One case in which this could apply is when thermosets that are reinforced with continuous carbon fibres are being recycled, as the solvolysis approach could allow for a more effective separation of the fibres and the thermoset matrix. This recycling approach has already been demonstrated for dissociative, associative and degradable linkages.<sup>43-47</sup> Nevertheless, these composites could still benefit from the use

of a dissociative over an associative dynamic system, as part of the resin can be removed *via* a heat treatment which will reduce the amount of solvent used. The results obtained in this study do show that for short fibres and particulate composites, dynamic dissociative thermosets show even more potential. For these materials mechanical recycling can be performed in a similar fashion to thermoplastic composite products. The results in this study show that these recycling processes will be more difficult when associative thermosets are used as matrix materials. To further underline these conclusions it is recommended that future studies build on the present study, characterize the impact of recycling on the mechanical performance of these materials and investigate the recycling potential of these thermoset matrices once they are processed into composites with particles or fibres.

## 4. Conclusions

The potential to reprocess thermosets with dissociative and associative dynamic covalent linkages by applying a thermal stimulus was studied in a quantitative experimental way. Two near-identical model thermoset polymer networks were synthesized in which only the dynamic covalent linkage was altered. A DA linkage was introduced in order to obtain a dissociative thermoset material, while a VU linkage was selected to serve as the model associative system. In correspondence with earlier studies, it is shown that the dynamic behaviour upon the application of a thermal stimulus is highly dependent on the selected molecular mechanisms, *i.e.* the type of reversible bond. Due to the molecular similarity of the model thermoset systems it was possible to assess the thermal reprocessing potential of these mechanisms in a quantitative manner. It is shown that the viscosity of a thermoset containing dissociative linkages can be severely reduced by applying heat, which could allow for mechanical recycling and reprocessing into new products *via* thermoplastic processing techniques such as (cast) extrusion and injection moulding. A similar effect on the viscosity was not observed in the associative thermoset and therefore the potential to reprocess these materials *via* thermoplastic processing operations is anticipated to be lower compared to its dissociative counterpart. As the selected polymer backbones for these model molecular structures were deliberately chosen as small as possible in order to maximize the observed dynamic covalent response, the observed difference in the mechanical recycling potential may be smaller in more application oriented thermoset resins.

## Author contributions

Willem Vogelzang: conceptualization and investigation. Wouter Teunissen: investigation. Arijana Susa, Wouter Post and Evelien Maaskant: conceptualization, supervision and writing – original draft. Karin Molenveld writing – review and editing.



## Data availability

The authors confirm that the data supporting the findings of this study are available within the article and its ESI.†

## Conflicts of interest

The authors have no conflicts of interest to declare that are relevant to the contents of this article.

## Acknowledgements

This project has received funding from the Wageningen University Knowledge Base Programme: Towards a circular and climate positive society (project KB-34-011-001: Recycling and end-of-life strategies for sustainability and climate) that is supported by finance from the Dutch Ministry of Agriculture, Nature and Food Quality. The project has also received funding from the European Union's Horizon Europe Research and Innovation program under agreement no. 101058371.

## References

- 1 N. Zhong and W. Post, Self-repair of structural and functional composites with intrinsically self-healing polymer matrices: A review, *Composites, Part A*, 2015, **69**, 226–239.
- 2 W. Post, *et al.*, A Review on the Potential and Limitations of Recyclable Thermosets for Structural Applications, *Polym. Rev.*, 2020, 359–388.
- 3 G. Oliveux, L. O. Dandy and G. A. Leeke, Current status of recycling of fibre reinforced polymers: Review of technologies, reuse and resulting properties, *Prog. Mater. Sci.*, 2015, **72**, 61–99.
- 4 S. J. Pickering, Recycling technologies for thermoset composite materials-current status, *Composites, Part A*, 2006, **37**(8), 1206–1215.
- 5 S. M. Al-Salem, *et al.*, A review on thermal and catalytic pyrolysis of plastic solid waste (PSW), *J. Environ. Manage.*, 2017, **197**, 177–198.
- 6 F. Snijkers, R. Pasquino and A. Maffezzoli, Curing and viscoelasticity of vitrimers, *Soft Matter*, 2017, **13**(1), 258–268.
- 7 F. García and M. M. J. Smulders, Dynamic covalent polymers, *J. Polym. Sci., Part A: Polym. Chem.*, 2016, **54**(22), 3551–3577.
- 8 Y.-L. Liu and T.-W. Chuo, Self-healing polymers based on thermally reversible Diels–Alder chemistry, *Polym. Chem.*, 2013, **4**(7), 2194–2205.
- 9 T. Ikezaki, *et al.*, Biobased poly(2,5-furandimethylene succinate-co-butylene succinate) crosslinked by reversible Diels–Alder reaction, *J. Polym. Sci., Part A: Polym. Chem.*, 2014, **52**(2), 216–222.
- 10 W. Post, *et al.*, Healing of a glass fibre reinforced composite with a disulphide containing organic-inorganic epoxy matrix, *Compos. Sci. Technol.*, 2017, **152**, 85–93.
- 11 M. Pepels, *et al.*, Self-healing systems based on disulfide–thiol exchange reactions, *Polym. Chem.*, 2013, **4**(18), 4955–4965.
- 12 X. Lei, *et al.*, Rehealable imide–imine hybrid polymers with full recyclability, *J. Mater. Chem. A*, 2017, **5**(40), 21140–21145.
- 13 P. Taynton, *et al.*, Repairable woven carbon fiber composites with full recyclability enabled by malleable polyimine networks, *Adv. Mater.*, 2016, **28**(15), 2904–2909.
- 14 D. A. Kissounko, P. Taynton and C. Kaffer, New material: vitrimers promise to impact composites, *Reinf. Plast.*, 2018, **62**(3), 162–166.
- 15 W. Denissen, J. M. Winne and F. E. Du Prez, Vitrimers: permanent organic networks with glass-like fluidity, *Chem. Sci.*, 2016, **7**(1), 30–38.
- 16 F. Van Lijsebetten, *et al.*, A Highly Dynamic Covalent Polymer Network without Creep: Mission Impossible?, *Angew. Chem., Int. Ed.*, 2022, **61**(48), e202210405.
- 17 W. Denissen, J. M. Winne and F. E. Du Prez, Vitrimers: permanent organic networks with glass-like fluidity, *Chem. Sci.*, 2016, **7**(1), 30–38.
- 18 D. Montarnal, *et al.*, Silica-Like Malleable Materials from Permanent Organic Networks, *Science*, 2011, **334**(6058), 965–968.
- 19 C. N. Bowman and C. J. Kloxin, Covalent Adaptable Networks: Reversible Bond Structures Incorporated in Polymer Networks, *Angew. Chem., Int. Ed.*, 2012, **51**(18), 4272–4274.
- 20 B. Krishnakumar, *et al.*, Vitrimers: Associative dynamic covalent adaptive networks in thermoset polymers, *Chem. Eng. J.*, 2020, **385**, 123820.
- 21 M. Maaz, *et al.*, Synthesis of Polyethylene Vitrimers in a Single Step: Consequences of Graft Structure, Reactive Extrusion Conditions, and Processing Aids, *Macromolecules*, 2021, **54**(5), 2213–2225.
- 22 M. Röttger, *et al.*, High-performance vitrimers from commodity thermoplastics through dioxaborolane metathesis, *Science*, 2017, **356**(6333), 62–65.
- 23 A. Breuillac, A. Kassalias and R. Nicolaï, Polybutadiene vitrimers based on dioxaborolane chemistry and dual networks with static and dynamic cross-links, *Macromolecules*, 2019, **52**(18), 7102–7113.
- 24 F. Caffy and R. Nicolaï, Transformation of polyethylene into a vitrimer by nitroxide radical coupling of a bis-dioxaborolane, *Polym. Chem.*, 2019, **10**(23), 3107–3115.
- 25 A. Breuillac, *et al.*, Functionalization of polyisoprene and polystyrene via reactive processing using azidoformate grafting agents, and its application to the synthesis of dioxaborolane-based polyisoprene vitrimers, *Polym. Chem.*, 2020, **11**(40), 6479–6491.
- 26 M. Guerre, *et al.*, Fluorinated Vitrimer Elastomers with a Dual Temperature Response, *J. Am. Chem. Soc.*, 2018, **140**(41), 13272–13284.
- 27 S. Hayashi, *et al.*, Synthesis and cross-linking behavior of biobased polyesters composed of bi(furfuryl alcohol), *Eur. Polym. J.*, 2019, **121**, 109333.



28 E. Galbis, *et al.*, Tandem ATRP/Diels–Alder synthesis of polyHEMA-based hydrogels, *Polym. Chem.*, 2014, **5**(18), 5391–5402.

29 F. Van Lijsebetten, *et al.*, Masked Primary Amines for a Controlled Plastic Flow of Vitrimers, *ACS Macro Lett.*, 2022, **11**(7), 919–924.

30 W. Denissen, *et al.*, Vinylogous Urethane Vitrimers, *Adv. Funct. Mater.*, 2015, **25**(16), 2451–2457.

31 A. Duval, *et al.*, Biobased and Aromatic Reversible Thermoset Networks from Condensed Tannins via the Diels–Alder Reaction, *ACS Sustainable Chem. Eng.*, 2017, **5**(1), 1199–1207.

32 G. Fortunato, *et al.*, Simultaneous Recovery of Matrix and Fiber in Carbon Reinforced Composites through a Diels–Alder Solvolysis Process, *Polymers*, 2019, **11**(6), 1007.

33 Y. Yang, *et al.*, Detecting topology freezing transition temperature of vitrimers by AIE luminogens, *Nat. Commun.*, 2019, **10**, 3165.

34 K. Roos, *et al.*, Activated anionic ring-opening polymerization for the synthesis of reversibly cross-linkable poly(propylene oxide) based on furan/maleimide chemistry, *Polym. Chem.*, 2016, **7**(8), 1612–1622.

35 D. Ehrhardt, *et al.*, Self-Healing in Mobility-Restricted Conditions Maintaining Mechanical Robustness: Furan–Maleimide Diels–Alder Cycloadditions in Polymer Networks for Ambient Applications, *Polymers*, 2020, **12**(11), 2543.

36 L. A. Pothan, Z. Oommen and S. Thomas, Dynamic mechanical analysis of banana fiber reinforced polyester composites, *Compos. Sci. Technol.*, 2003, **63**(2), 283–293.

37 A. Susa, *et al.*, Understanding the Effect of the Dianhydride Structure on the Properties of Semiaromatic Polyimides Containing a Biobased Fatty Diamine, *ACS Sustainable Chem. Eng.*, 2018, **6**(1), 668–678.

38 A. Jourdain, *et al.*, Rheological Properties of Covalent Adaptable Networks with 1,2,3-Triazolium Cross-Links: The Missing Link between Vitrimers and Dissociative Networks, *Macromolecules*, 2020, **53**(6), 1884–1900.

39 S. Seghers, *et al.*, Improving the efficiency of the Diels–Alder process by using flow chemistry and zeolite catalysis, *Green Chem.*, 2017, **19**(1), 237–248.

40 F. Orozco, *et al.*, Maleimide Self-Reaction in Furan/Maleimide-Based Reversibly Crosslinked Polyketones: Processing Limitation or Potential Advantage?, *Molecules*, 2021, **26**(8), 2230.

41 J. Vlachopoulos and D. Strutt, *The Role of Rheology in Polymer Extrusion*. Extrusion Minitec and Conference: From Basics to Recent Developments, 2003.

42 E. Maaskant and W. Post, Recyclable Thermoset Polymer Composites Based on Degradable and Dynamic Covalent Chemistry, in *Reference Module in Materials Science and Materials Engineering*, Elsevier, 2021.

43 S. L. Buchwalter and L. L. Kosbar, Cleavable epoxy resins: Design for disassembly of a thermoset, *J. Polym. Sci., Part A: Polym. Chem.*, 1996, **34**(2), 249–260.

44 T. Hashimoto, *et al.*, Degradable and chemically recyclable epoxy resins containing acetal linkages: Synthesis, properties, and application for carbon fiber-reinforced plastics, *J. Polym. Sci., Part A: Polym. Chem.*, 2012, **50**(17), 3674–3681.

45 S. Ma and D. C. Webster, Degradable thermosets based on labile bonds or linkages: A review, *Prog. Polym. Sci.*, 2018, **76**, 65–110.

46 M. Lejeail and H. R. Fischer, Development of a completely recyclable glass fiber-reinforced epoxy thermoset composite, *J. Appl. Polym. Sci.*, 2020, 49690.

47 M. Lejeail and H. R. Fischer, Investigations on the replacement of bismaleimide by the bio-based bisitaconimide for recyclable thermoset composites based on thermo-reversible Diels–Alder cross-links, *Eur. Polym. J.*, 2020, **131**, 109699.

